Fisher, L. E., Yang, Y., Yuen, M-F., Zhang, W., Nobbs, A. H., & Su, B. (2016). Bactericidal activity of biomimetic diamond nanocone surfaces. *Biointerphases*, *11*(1), [011014]. https://doi.org/10.1116/1.4944062

Biointerphases
A Journal of Biomaterials and Biological Interfaces

Bactericidal activity of biomimetic diamond nanocone surfaces

Leanne E. Fisher, Yang Yang, Muk-Fung Yuen, Wenjun Zhang, Angela H. Nobbs, and Bo Su

Citation: Biointerphases **11**, 011014 (2016); doi: 10.1116/1.4944062
View online: http://dx.doi.org/10.1116/1.4944062
View Table of Contents: http://scitation.aip.org/content/avs/journal/bip/11/1?ver=pdfcov
Published by the AVS: Science & Technology of Materials, Interfaces, and Processing

Bactericidal activity of biomimetic diamond nanocone surfaces

Leanne E. Fisher[a)]
School of Oral and Dental Sciences, University of Bristol, Bristol BS1 2LY, United Kingdom

Yang Yang, Muk-Fung Yuen, and Wenjun Zhang
Center of Super-Diamond and Advanced Films (COSDAF), and Department of Physics and Materials Science, City University of Hong Kong, Tat Chee Avenue, Kowloon, Hong Kong, China

Angela H. Nobbs and Bo Su
School of Oral and Dental Sciences, University of Bristol, Bristol BS1 2LY, United Kingdom

(Received 15 January 2016; accepted 3 March 2016; published 17 March 2016)

The formation of biofilms on implant surfaces and the subsequent development of medical device-associated infections are difficult to resolve and can cause considerable morbidity to the patient. Over the past decade, there has been growing recognition that physical cues, such as surface topography, can regulate biological responses and possess bactericidal activity. In this study, diamond nanocone-patterned surfaces, representing biomimetic analogs of the naturally bactericidal cicada fly wing, were fabricated using microwave plasma chemical vapor deposition, followed by bias-assisted reactive ion etching. Two structurally distinct nanocone surfaces were produced, characterized, and the bactericidal ability examined. The sharp diamond nanocone features were found to have bactericidal capabilities with the surface possessing the more varying cone dimension, nonuniform array, and decreased density, showing enhanced bactericidal ability over the more uniform, highly dense nanocone surface. Future research will focus on using the fabrication process to tailor surface nanotopographies on clinically relevant materials that promote both effective killing of a broader range of microorganisms and the desired mammalian cell response. This study serves to introduce a technology that may launch a new and innovative direction in the design of biomaterials with capacity to reduce the risk of medical device-associated infections. © *2016 American Vacuum Society*. [http://dx.doi.org/10.1116/1.4944062]

I. INTRODUCTION

The use of medical devices has become an essential part of modern day medicine and over the past few years the healthcare setting has seen a vast increase in their use. The diversity of such devices is wide, varying from those of a complex nature like automatic implantable cardio defibrillators to simpler devices such as urinary catheters.[1,2] While medical devices have improved clinical outcomes for patients, one thing biomaterials all have in common is their susceptibility to bacterial colonization. This can lead to the formation of biofilms on the material surface and subsequent medical device-associated infection.[3] A biofilm is an accumulation of microorganisms on a surface, embedded within an extracellular matrix, which together form a functional, structured community[4] that maximizes microbial survival.[5] Biofilm-associated infections of medical implants are difficult to resolve and can cause considerable morbidity to the patient. Microbial cells embedded within the depths of biofilms are protected from host defences and to the effects of antibiotics. Studies have shown that some microorganisms within biofilms require a >1000-fold higher concentration of antibiotics to be killed compared to their planktonic counterparts.[6] Revision surgery or device removal is often necessary to resolve the infection, and this can be at a considerable cost to the National Health Service and patient well-being.

There is therefore great incentive to devise strategies to minimize biofilm formation on medical devices and associated equipment. However, materials completely resistant to bacterial colonization for clinically significant periods currently remain elusive. Over the past decade there has been growing recognition that physical cues can regulate biological responses.[7] In an era of increasing antibiotic resistance, physical-derived solutions to control bacterial colonization by modification of existing implant materials presents a promising and attractive alternative to antimicrobial agents or chemical based surface treatments. Of particular interest is the influence that surface topography (at both nano- and microscale) has on bacterial viability, and a better understanding as to which and how nano/microfeatures may be exploited to prevent implant-associated infection is required.

Two of the most widely studied physical-based strategies for antimicrobial surfaces using micro-[8,9] or nanotopographies[10–13] are inhibition of microbial attachment (antibiofouling) or contact-killing. An example of an antibiofouling surface is the Sharklet micropattern surface, inspired by shark skin.[14] When patterned onto endotracheal tubes, it was found to inhibit attachment of numerous pathogens by up to 99% compared to unpatterned controls, and also inhibited the formation of methicillin-resistant *Staphylococcus aureus* and *Pseudomonas aeruginosa* biofilms.[15] The first biomimetic surface shown to directly kill bacteria upon contact was recently described by Ivanova.[11] The cicada (*Psaltoda claripennis*) fly wing possesses nanofeatures that consist of

[a)]Electronic mail: l.e.fisher@bristol.ac.uk

hexagonal arrays of spherically capped, conical, nanoscale pillars, which are typically 200 nm tall, 100 nm in diameter at the base, 60 nm in diameter at the cap, and spaced 170 nm apart from center to center.[11,16] When generated on titanium, these features were shown to be extremely effective at killing *P. aeruginosa* and this was proposed to be due to a mechanical based mechanism, whereby bacterial cell walls were stretched and punctured by the nanospikes, resulting in cell death. The same group also investigated the antibacterial potential of structures found on the wings of dragonfly *Diplacodes bipunctata* and of a black silicon synthetic biomimetic analog.[17] The high aspect ratio nanoprotrusions on both surfaces were found to be highly bactericidal against both Gram negative and Gram positive bacteria, with kill rates of up to 450 000 cells $min^{-1} cm^{-2}$.[17] Likewise, Diu[9] engineered cicada wing-inspired nanowire topographies on medically relevant titanium surfaces using an alkaline hydrothermal process as a function of time. They reported bactericidal activity that was particularly effective against Gram negative motile bacterial cells.

Cicada wing features have been reported as displaying a nanopillar morphology;[11,18] however, careful observation by a scanning electron microscopy (SEM) shows that they more closely resemble nanocone structures, since the base of the structure is wider than its tip.[19,20] Previous work by Chong[21] and Yang[22,23] has demonstrated fabrication of arrays of high-aspect-ratio diamond nanocones and nanoneedles. These nanocone arrays were found to mechanically puncture mouse MC3T3-E1 preosteoblast cells, which aided the delivery of molecules into the cells.[21] However, the arrays were not tested for their ability to damage more rigid bacterial cell walls. Herein, we report the production and bactericidal activity of diamond nanocone-patterned surfaces and show their ability to reduce microbial viability of the Gram negative opportunistic pathogen *P. aeruginosa*, a common causative agent of medical device-associated infections.

II. EXPERIMENT

A. Fabrication of diamond nanocone arrays

Nanocone fabrication was based upon two processes, as previously described.[23] First diamond films were deposited by microwave plasma chemical vapor deposition (MPCVD), followed by bias-assisted reactive ion etching (RIE) by electron cyclotron resonance (ECR) mode microwave plasma. Polycrystalline films were first deposited on substrates [an n-type (001) silicon wafer], using a commercial ASTeX MPCVD equipped with a 1.5 kW microwave generator. Prior to film deposition, the substrates were scratched using 0.25 nm diamond particle paste. The polycrystalline film deposition was performed in the plasma induced in a 0.5% CH_4/H_2 mixture at a total pressure of 30 Torr and a total gas-flow rate of 300 sccm. The microwave was maintained at 1200 W and the substrate temperature measured by optical pyrometer was kept at approximately 850 °C. After the nanodiamond film deposition was finished, the second step of RIE was performed using ECR mode microwave plasma. The ASTeX microwave source employed a magnetic field of about 875 Gauss generated by an external magnetic coil. The RIE conditions were as follows: A mixture of 45% Ar/55% H_2 was used as the reactive gases at a total flow rate of 20 sccm; the substrate bias was of −150 to −200 V; the reactant pressure was 1.0×10^{-3} Torr. The etching duration was 2 h, and the input microwave power was 1400 W.

Two diamond nanocone surfaces were fabricated and cut into 5 × 5 mm squares. Surface A, which was obtained when the RIE bias was −200 V, and surface B, which was obtained when the RIE bias was −150 V. The approximate morphology of the diamond nanocone patch was characterized using scanning electron microscopy by tilting the sample holder with a 45° angle.

B. Bacterial culture preparation

P. aeruginosa ATCC 27853 was grown aerobically for 16 h in 10 ml Luria–Bertani broth (LBB, Sigma Aldrich) in a 37 °C shaker incubator set at 220 rpm. The bacterial suspension was then diluted in LBB to OD_{600} 0.1 and further incubated until midexponential phase was reached. At this time bacterial cells were harvested by centrifugation (7 min, 5000 *g*), washed twice in 10 mM Tris-HCl buffer (Sigma Aldrich), and suspended in Tris-HCl buffer to OD_{600} 0.3 (approx. 10^7 cfu ml^{-1}).

C. Bacterial adhesion

All test and control surfaces were rinsed with absolute ethanol prior to bacterial adhesion experiments. The test surfaces and controls were placed into a 12-well microtiter plate and submerged in 2 ml of bacterial suspension. Plates were incubated for 1 h at 37 °C under static conditions. After incubation, surfaces were rinsed to remove nonadherent bacteria by gently holding the surfaces with a pair of tweezers and passing back and forth five times in a uniform manner into a Universal container containing Tris-HCl buffer. The process was repeated three times in total.

D. Live/Dead staining and fluorescence microscopy

Following rinsing, 1 ml of Live/Dead® BacLight™ bacterial viability stain (Invitrogen) was applied to the surfaces (as per manufacturers' instructions) and incubated in the dark for 15 min at room temperature. Surfaces were then rinsed in Tris-HCl buffer as above to remove excess stain. Surfaces were maintained in 1 ml of Tris-HCl buffer, and bacterial adhesion and viability was visualized by fluorescence microscopy. IMAGE J software was used to calculate the number of cells with intact membranes (SYTO 9, green) and the number of cells with damaged membranes (propidium iodide, red) based on five images per surface. The average percentage damaged cells was determined by (no. of damaged cells/total no. of cells) × 100. All tests were carried out in triplicate. A two tailed homoscedastic Student's t-test was performed using Microsoft Excel 2013 to compare data sets. If the p value was less than 0.05, then results were statistically significant.

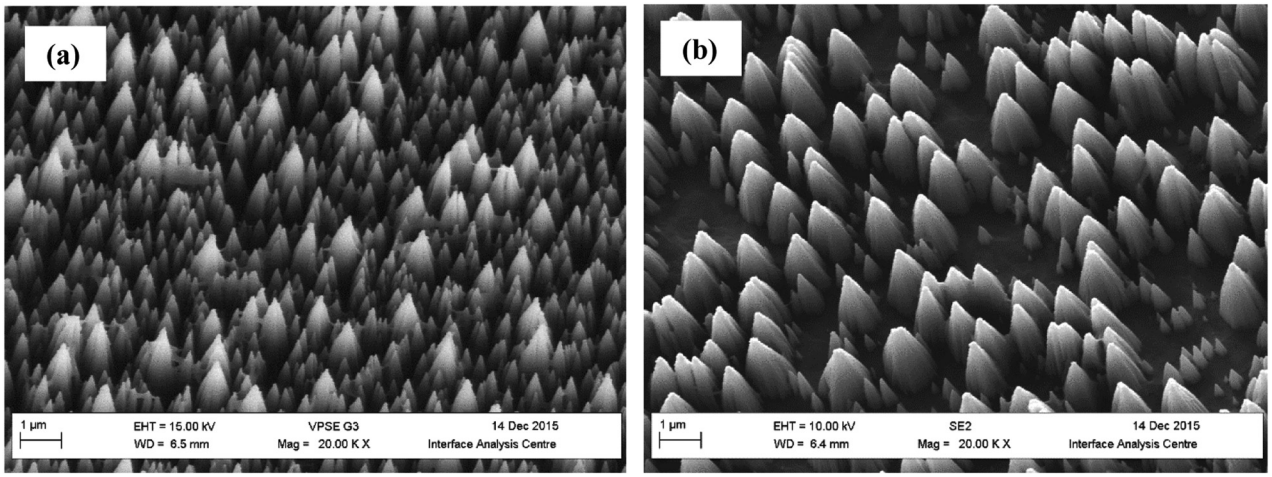

FIG. 1. SEM images of (a) surface A diamond cone nanopatterned silicon wafer and (b) surface B diamond cone nanopatterned silicon wafer generated by ECR-assisted plasma RIE.

E. Scanning electron microscopy

Following incubation with *P. aeruginosa*, surfaces were fixed by immersion in a 2.5% gluteraldehyde solution (Sigma Aldrich) dissolved in 0.1 M potassium phosphate buffer (potassium phosphate monobasic and potassium phosphate dibasic, *p*H 7.2, Sigma Aldrich) for 2 h at room temperature. An alcohol dehydration stage was then performed by immersing the surfaces in 20%, then 40%, 60%, 80%, and 100% ethanol for 10 min each prior to 10 min in hexamethyldisilazane (Sigma Aldrich). Surfaces were then air dried, mounted onto carbon stubs, and sputtered twice with gold for 1 min each time. A Helios Nanolab 600 combined with FIB-SEM was used to visualize the surfaces.

III. RESULTS AND DISCUSSION

A. Fabrication of diamond nanocone arrays

In this study, high-density diamond nanocone arrays were successfully prepared by ECR-assisted plasma RIE. The samples were tilted to a 45° angle toward the SEM detector for observation and the diamond nanocones displayed different sizes and heights, each with a sharp cone tip (Fig. 1). The height of the cones on surface A range from 800 nm to 2.5 μm, with the average height being about 1.65 μm. However, on surface B, the size of the diamond nanocones can be divided into two groups. A fraction of the diamond nanocones are very small, with heights of less than 100 nm. On the other hand, many of the diamond cones are very large in size, with heights in the range of 3–5 μm. The width of the cones ranged from 350 to 750 nm on surface A and $<$100 nm to 1.2 μm on surface B. Both surfaces displayed sharp tips which ranged from 10 to 40 nm and surface B was shown to display greater spacing between the cones compared to surface A. On surface A, the diamond nanocones are intensively alligned with a density of $\sim 4 \times 10^8/\text{cm}^2$ while the distribution density on surface B was smaller at $1.7 \times 10^8/\text{cm}^2$, as determined by counting the nanocones in several representative SEM images. The two surfaces appeared a uniformly black color due to the antireflective property of the high density diamond nanocones distributed over the entire substrate surface.

The phase composition of the nanocones was studied using visible Raman spectroscopy and the Raman spectra of the pristine microcrystalline diamond film and the diamond nanocone array film are plotted in Fig. 2, after linear background removal and normalization to the characteristic peak of diamond at 1332 cm^{-1}. The microcrystalline diamond film exhibit Raman bands at about 1350 and 1500 cm^{-1} attributed to amorphous carbon. After etching, the band at 1350 cm^{-1}, associated with disordered amorphous carbon nearly disappeared. On the other hand, the band at 1500 cm^{-1} decreased its intensity and broadened. Thus, the diamond nanocones formed by reactive ion etching retained the microstructure of the microcrystalline diamond film but had less graphite and amorphous carbon phase. The ECR-assisted plasma RIE involves the physical etching by

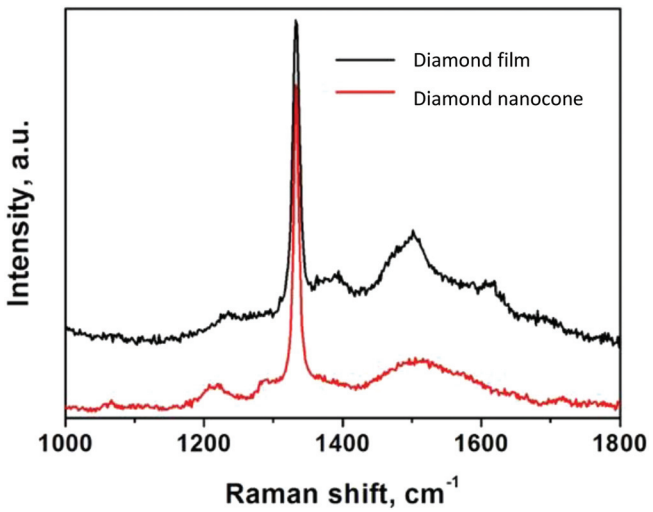

FIG. 2. Raman spectrum obtained from pristine microcrystalline diamond film and microcrystalline diamond nanocone arrays.

energetic ion impact and the chemical etching of graphite or amorphous carbon by reactive hydrogen atoms/ions. The inhomogeneous distribution of electrical field in the reactive plasma causes the preferential etching of graphite and amorphous carbon in the grain boundary regions of the microcrystalline diamond film by either physical or chemical sputtering. Consequently, the graphite and amorphous carbon phase decreased in the fabricated diamond nanocone arrays film.

B. Topographical effect on bacterial adhesion and viability

To date, a variety of diamond nanostructured arrays such as nanocones, nanowires, nanopillars, or nanowhiskers have been produced for application in the field of energy, electronics, and biosensing.[23] However, there are no reports on the effects of biomimetic diamond nanocone-patterned surfaces on bacterial viability. *P. aeruginosa* is a highly motile, rod-shaped, aerobic, Gram negative bacterium, and is the fifth most common organism isolated from all sites of nosocomial infection.[24] It grows in biofilms that promote growth and survival within the human body and on medical implants such as catheters or on orthopedic, respiratory, or cardiac devices and is inherently resistant to many antibiotics. Previous studies have observed that certain nanostructures have a greater bactericidal effect against Gram negative bacterial cells than Gram positive cells.[9,11,18] The reasoning for this is postulated as relating to the thickness of the bacterial cell wall. Most Gram positive bacteria have relatively thick cell walls with a peptidoglycan layer of approximately 20–80 nm, whereas the peptidoglycan layer in Gram negative cell walls is much thinner (about 5–10 nm).[25] Thus, it has been suggested that Gram negative bacteria require less stress to disrupt the cell wall, resulting in a greater extent of cell death than seen with Gram positive cells. Furthermore, it has been reported that bacterial motility may be associated with a more pronounced bactericidal effect.[9] For these reasons, *P. aeruginosa* was used as a model bacterium to test the bactericidal efficacy of the diamond nanocone-patterned surfaces.

Both surfaces A and B were exposed to high numbers of exponential phase *P. aeruginosa* for 1 h and their bactericidal effects assessed using Live/Dead staining. Typical fluorescence micrographs are shown in Fig. 3, in which cells with intact membranes are stained green and cells with damaged membranes are stained red. While concerns have recently been raised regarding *P. aeruginosa* cells having a stronger dead cell (propidium iodide) signal than the live cells (SYTO 9), in a separate experiment involving staining exponential phase cells and stationary phase cells (data not shown), cells in the exponential phase of growth and as performed in our adhesion assay show almost all live stained cells. This is in direct contrast to the many nonviable or dead cells in stationary phase culture. Both nanopatterned surfaces showed a significantly ($p < 0.001$) higher proportion of membrane damaged cells with very few red cells present on flat control surfaces, underscoring the fact that the nanofeatures were responsible for the killing effects. Furthermore, while cells attached to the control surface were aligned on the horizontal plane, bacterial cells associated with either nanopatterned surface were visualized in different orientations, suggesting that they positioned themselves both across the diamond cone tips and were retained vertically in between the cone structures. This was seen with both viable and nonviable cells and an example of this is shown by the arrow in Fig. 3(c), whereby cells orientate themselves with their ends facing upwards.

The nanopatterned surfaces tested in this study found comparable numbers of cells as the control silicon wafer ($p > 0.05$) [Fig. 4(a)]. However, research regarding the capacity for nanopatterned surfaces to attract bacterial attachment is contradictory. Dickson[10] found that lower cell densities were retained on PMMA pillared surfaces following 20 h culture compared to on flat surfaces. In contrast, other research findings have illustrated that the presence of nanofeatures can promote bacterial adhesion.[8,26] Such differences may be linked to the interplay of different physicochemical properties of the material features, bacterial strains tested and culture techniques, or environmental conditions. Nonetheless, what is clear in this study is that while the

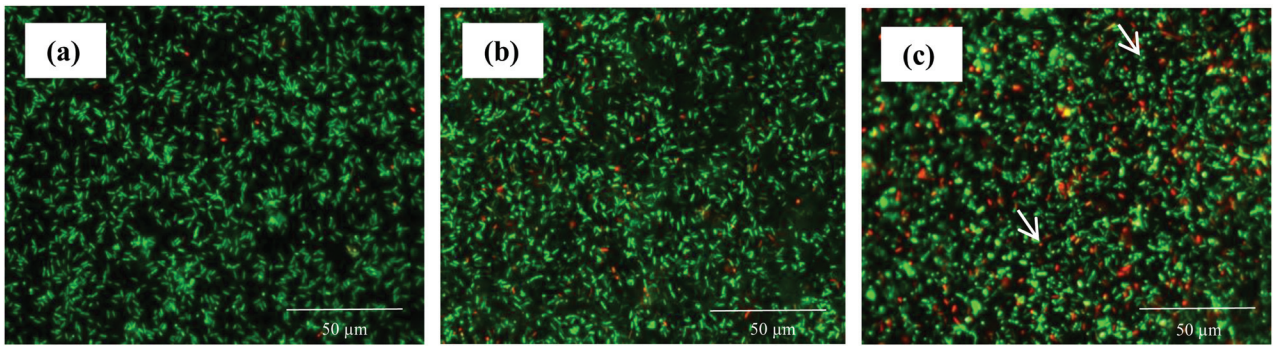

FIG. 3. Fluorescence micrographs of *P. aeruginosa* after 1 h incubation on (a) control silicon wafer, (b) surface A diamond cone nanopatterned silicon wafer or (c) surface B diamond cone nanopatterned silicon wafer. Bacterial viability Live/Dead BacLight assays stained cells with intact membranes green (SYTO 9) and cells with damaged membranes red (propidium iodide). Surface B, for example, (c) as indicated by the arrows, shows cells aligned with their ends facing upwards in addition to lying horizontally.

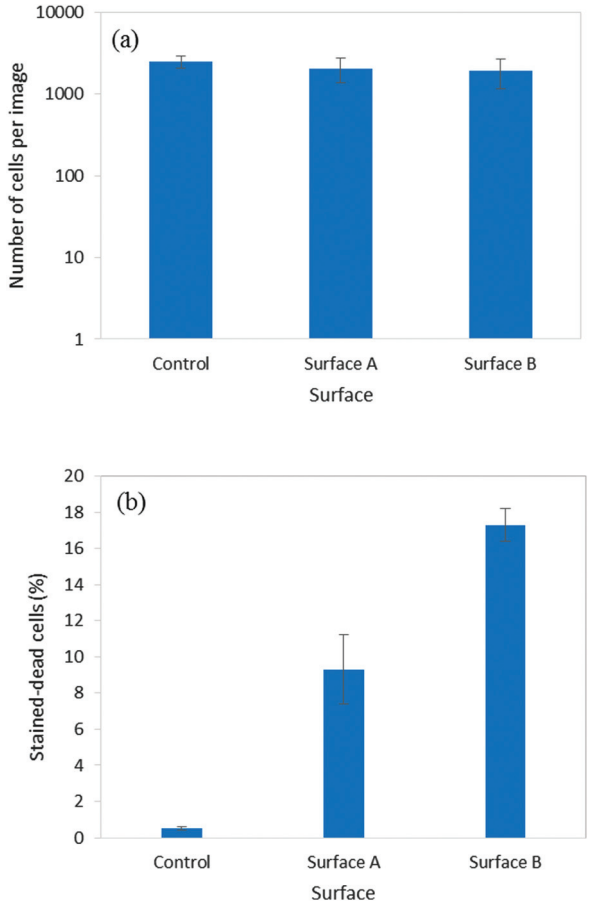

FIG. 4. Total numbers of bound bacteria (a) and percentage dead cells (b) after 1 h incubation of *P. aeruginosa* on control silicon wafer, surface A diamond cone nanopatterned silicon wafer, or surface B diamond cone nanopatterned silicon wafer, and subsequent viability determination by Live/Dead BacLight stain.

diamond nanocone surfaces may be bound by bacteria, this bacterial attachment results in significant killing of the deposited bacterial population.

The percentage of stained-dead cells on surface A and surface B compared to the control is shown in Fig. 4(b). Both of the nanopatterned surfaces resulted in significant bacterial killing compared to the control (<0.05%), with surface B displaying significantly ($p = 0.006$) greater bactericidal activity (17% killing) than surface A. Due to the higher ion bombardment by increasing the reactive ion etching bias to −200 V, nanocones formed on surface A showed sharp tips, higher cone density, and were more homogeneous in size compared with those formed by bias of −150 V on surface B. While no in depth study of nanocone size in relation to bacterial cell interaction is reported, it would appear the size variation, nonuniformity and the decreased cone density of nanocone arrays on surface B may act in a way to facilitate its bactericidal activity. In a mathematical model by Xue[27] explaining the mechanism of the bactericidal properties of the cicada wing, they suggest that when nanofeatures become sharper and the spacing between them is larger, the antibacterial properties of the surface are enhanced. Nowlin[28] also report that nanopillars with the smallest diameters were able to kill even the weakest adhering strain of *Saccharomyces cerevisiae*. This supports the findings from percentage kill differences between the nanocone features on surfaces A and B. In contrast a study by Kelleher,[20] suggests that the greater the number of nanostructures with which bacterial cells come into contact, the greater the bactericidal activity; however, they do also state this could be related to the nanostructure pitch and diameter of the features.

In addition to viability staining, equivalent samples were also fixed after the 1 h bacterial adhesion for visualization by SEM, as shown in Fig. 5. Images revealed horizontally positioned, healthy (turgid) cells on the flat control surfaces [Fig. 5(a)], correlating with the appearance of those samples visualized by fluorescence microscopy. It was hypothesized that bacterial contact with the sharp, nanometer-sized tips of the diamond nanocones would generate stress forces across the bacterial cell wall, causing cells to stretch and puncture and ultimately lyse, resulting in cell death. *P. aeruginosa* adhering to the densely packed cones of surface A which had slight differences in height and width, but each with sharp nanometer-sized tips was shown to settle both on top of these cones and at angles in between the cones [Fig. 5(b)]. Many of the cells [false-colored in Fig. 5(b)] appeared to

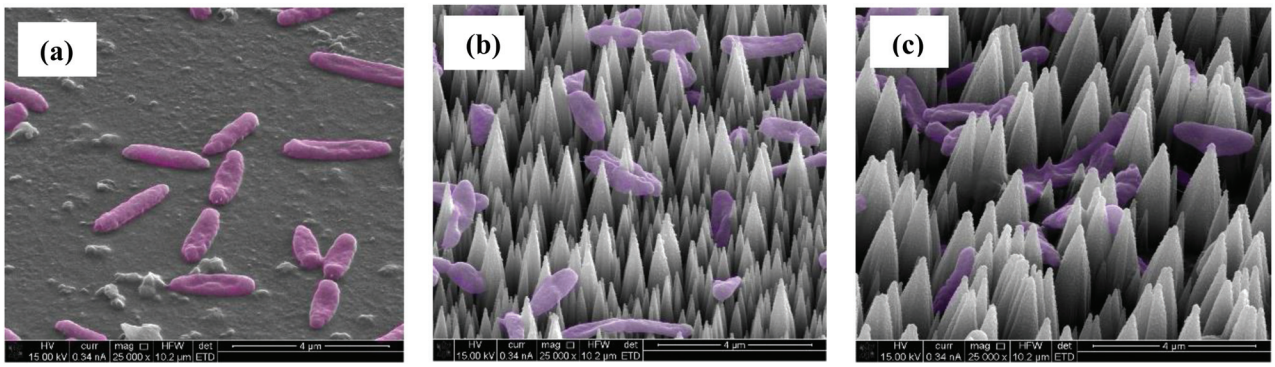

FIG. 5. Example SEM images of *P. aeruginosa* after 1 h incubation on (a) control silicon wafer, (b) surface A diamond cone nanopatterned silicon wafer or (c) surface B diamond cone nanopatterned silicon wafer. Image (a) shows healthy (turgid) bacterial cells, whereas images (b) and (c) show some damaged cells that have been spiked or punctured by the diamond nanocone features.

display an undamaged morphology. However, a proportion appeared to be damaged by the nanofeatures. The more notable differences in cone size, height, width and spacing on surface B showed the *P. aeruginosa* cells to lie across the tops of the cones, fall in between them or attach directly to the flat surface in between the cones [false-colored in Fig. 5(c)]. Nonetheless, the greater nonuniformity of this surface appeared to effectively damage a higher percentage of cells as also reported from Live/Dead assays. Collapse and spreading of these cells over the features was visible, indicative of nonrecoverable cell death.

The diamond nanocone-shaped features were successfully shown to possess bactericidal capabilities and thus to have potential to reduce bacterial contamination of medical devices. In order to provide scope to investigate the optimal feature specifications to achieve maximum bacterial killing, it is important for the fabrication technique to be tuneable,[29] as is the case here. With further modification it will be possible to generate diamond nanocone features that exhibit a greater kill efficacy. Topographical feature shape and size, along with distribution and spacing in relation to the size and shape of the bacteria, are undoubtedly key elements to consider when engineering nanopatterned surfaces.

While the nanopatterned surfaces serve to enhance bacterial killing, they should also support human cell adhesion, differentiation, and thus integration with human tissues. For example, integration between living bone and a hip or tooth implant (osteointegration) is essential for implant-host survival and thus implant longevity.[30] Kalbacova[31] investigated osteoblast adhesion to diamond nanorod and nanocone structures, and found osteoblasts seeded onto these surfaces formed focal adhesion patterns, indicating the suitability of the surface structures to support cell adhesion, growth, and differentiation. Thus, the ECR-assisted plasma RIE fabricated diamond nanocone surfaces must also be tested for promotion of human cell proliferation while at the same time exhibiting bactericidal capabilities.

IV. CONCLUSIONS

Diamond nanocone-patterned surfaces, representing biomimetic analogs of the cicada fly wing, were fabricated using an ECR-assisted plasma RIE process. Both surfaces A and B were found to possess bactericidal capabilities, with surface B displaying a higher kill rate. To be applied within the medical setting, future research will need to demonstrate that the technique can be used to tailor surface nanotopographies on clinically relevant materials (e.g., titanium) that promote both a desired mammalian cell response and effective killing of a broader range of microorganisms. Nonetheless, this study serves to introduce a technology that may launch a new and innovative direction in the design of biomaterials with capacity to reduce the risk of medical device-associated infections.

ACKNOWLEDGMENTS

The authors wish to thank the financial support from the EPSRC (EP/K035142/1). SEM studies were carried out in the Chemical Imaging Facility, University of Bristol with equipment funded by EPSRC under Grant "*Atoms to Applications*" (EP/K035746/1).

[1]M. Ghannoum and G. O'Toole, *Microbial Biofilms* (ASM, Washington, DC, 2004).
[2]K. Anselme, P. Davidson, A. M. Popa, M. Giazzon, M. Liley, and L. Ploux, Acta Biomater. **6**, 3824 (2010).
[3]E. Hart *et al.*, J. Antimicrob. Chemother. **65**, 974 (2010).
[4]P. Tenke, C. R. Riedl, G. L. Jones, G. J Williams, D. Stickler, and E. Nagy, Int. J. Antimicrob. Agents **23**, 67 (2004).
[5]P. A. Cadieux, G. R. Wignall, R. Carriveau, and J. D. Denstedt, *Renal Stone Disease 2*, AIP Conference Proceedings Vol. 1049, edited by A. P. Evan, J. E. Lingeman, J. A. McAteer, and J. C. Williams (Melville, New York, 2008), pp. 147–163.
[6]P. S. Stewart and J. W. Costerton, Lancet **358**, 135 (2001).
[7]S. Mitragotri and J. Lahann Nat. Mater. **8**, 15 (2009).
[8]K. A. Whitehead, J. Colligon, and J. Verran Colloid Surf., B **41**, 129 (2005).
[9]T. Diu, N. Faruqui, T. Sjostrom, B. Lamarre, H. F. Jenkinson, B. Su, and M. G. Ryadnov, Sci. Rep. **4**, 7122 (2014).
[10]M. N. Dickson, E. I. Liang, L. A. Rodriguez, N. Vollereaux, and A. F. Yee, Biointerphases **10**, 021010 (2015).
[11]E. P. Ivanova *et al.*, Small **8**, 2489 (2012).
[12]J. Pang, D. Dymock, T. Sjostrom, and B. Su Bioinspired, Biomimetic Nanobiomater. **2**, 117 (2013).
[13]E. P. Ivanova *et al.*, Nat. Commun. **4**, 2838 (2013).
[14]E. E. Mann, D. Manna, M. R. Mettetal, R. M. May, E. M. Dannemiller, K. K. Chung, A. B. Brennan, and S. T. Reddy, Antimicrob. Resist. Infect. Control **3**, 28 (2014).
[15]R. M. May, M. G. Hoffman, M. J. Sogo, A. E. Parker, G. A. O'Toole, and S. T. Reddy, Clin. Transl. Med. **3**, 8 (2014).
[16]S. Pogodin *et al.*, Biophys. J. **104**, 835 (2013).
[17]E. P. Ivanova *et al.*, Nat. Commun. **4**, 7 (2013).
[18]J. Hasan, H. K. Webb, V. K. Truong, S. Pogodin, V. A. Baulin, G. S. Watson, J. A. Watson, R. J. Crawford, and E. P. Ivanova, Appl. Microbiol. Biotechnol. **97**, 9257 (2013).
[19]G. Zhang, J. Zhang, G. Xie, Z. Liu, and H. Shao, Small **2**, 1440 (2006).
[20]S. M. Kelleher, O. Habimana, J. Lawler, B. O' Reilly, S. Daniels, E. Casey, and A. Cowley, ACS Appl. Mater. Interfaces (2015).
[21]E. Y. W. Chong, C. Y. P. Ng, V. W. Y. Choi, L. Yan, Y. Yang, W. J. Zhang, K. W. K. Yeung, X. F. Chen, and K. N. Yu, J. Mater. Chem. B **1**, 3390 (2013).
[22]B. He, Y. Yang, M. F. Yuen, X. F. Chen, C. S. Lee, and W. J. Zhang, Nano Today **8**, 265 (2013).
[23]Y. Yang, M. F. Yuen, X. Chen, S. Xu, Y. Tang, and W. J. Zhang, Crystengcomm **17**, 2791 (2015).
[24]M. J. Richards, J. R. Edwards, D. H. Culver, and R. P. Gaynes, Crit. Care Med. **27**, 887 (1999).
[25]M. R. Salton and K.-S. Kim, *Medical Microbiology*, 4th ed. (University of Texas Medical Branch at Galveston, Galveston, TX, 1996).
[26]V. K. Truong, R. Lapovok, Y. S. Estrin, S. Rundell, J. Y. Wang, C. J. Fluke, R. J. Crawford, and E. P. Ivanova, Biomaterials **31**, 3674 (2010).
[27]F. Xue, J. Liu, L. Guo, L. Zhang, and Q. Li J. Theor. Biol. **385**, 1 (2015).
[28]K. Nowlin, A. Boseman, A. Covell, and D. LaJeunesse J. R. Soc. Interface **12**, 20140999 (2015).
[29]T. Sjostrom, A. S. Brydone, R. M. D. Meek, M. J. Dalby, B. Su, and L. E. McNamara, Nanomedicine **8**, 89 (2013).
[30]R. Branemark, P. I. Branemark, B. Rydevik, and R. R. Myers, J. Rehabil. Res. Dev. **38**, 175 (2001).
[31]M. Kalbacova, A. Broz, O. Babchenko, and A. Kromka Phys. Status Solidi B **246**, 2774 (2009).